A Model for the Rapid Assessment of Solution Structures for 24-Atom Macrocycles: The Impact of -Branched Amino Acids on Conformation

A Model for the Rapid Assessment of Solution-Structures for 24-Atom Macrocycles: The Impact of β-Branched Amino Acids on Conformation

Alexander J. Menke,[1] Camryn J. Gloor,[1] Liam E. Claton,[1] Magy A. Mekhail,[1] Hongjun Pan,[2] Mikaela D. Stewart,[3] Kayla N. Green,[1] Joseph H. Reibenspies,[4] Giovanni M. Pavan,[5,6] Riccardo Capelli,[7,*] and Eric E. Simanek[1,*]

riccardo.capelli@unimi.it

e.simanek@tcu.edu

[1]*Department of Chemistry & Biochemistry, Texas Christian University, Fort Worth TX 76129 USA*

[2]*Department of Chemistry, University of North Texas, Denton TX 76203 USA*

[3]*Department of Biology, Texas Christian University, Fort Worth TX 76129 USA*

[4]*Department of Chemistry, Texas A&M University, College Station TX 77845 USA*

[5]*Department of Innovative Technologies, University of Applied Sciences and Arts of Southern Switzerland, Polo Universitario Lugano, 6962 Lugano-Viganello, Switzerland*

[6]*Department of Applied Science and Technology, Politecnico di Torino, 10129 Torino, Italy*

[7]*Department of Biosciences, Università degli Studi di Milano, Via Celoria 26, 20133 Milan, Italy*

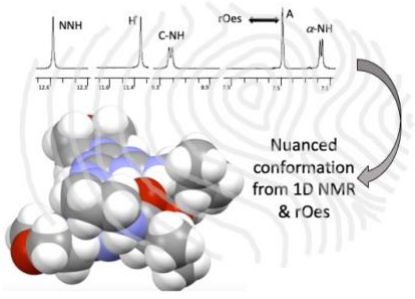

Abstract

Experiment and computation are used to develop a model to rapidly predict solution structures of macrocycles sharing the same Murcko framework. These 24-atom triazine macrocycles result from the quantitative dimerization of identical monomers presenting a hydrazine group and an acetal tethered to by an amino acid. Monomers comprising glycine and the β-branched amino acids threonine, valine, and isoleucine yield macrocycles **G-G**, **T-T**, **V-V**, and **I-I**, respectively. Elements common to all members of the framework include the efficiency of macrocyclization (quantitative), the solution- and solid-state structures (folded), the site of protonation (opposite the auxiliary dimethylamine group), the geometry of the hydrazone (*E*), the C2-symmetry of the subunits (conserved), and the rotamer state adopted. In aggregate, the data reveals metrics predictive of the 3-dimensional solution structure that derive from the fingerprint region of the 1D ^{1}H spectrum and a network of rOes from a single resonance. The metrics also afford delineation of more nuanced structural features that allow subpopulations to be identified amongst the members of the framework. Well-tempered metadynamics provides free energy surfaces and population distributions of these macrocycles. The areas of the free energy surface decrease with increasing steric bulk (**G-G** > **V-V** ~ **T-T** > **I-I**). In addition, the surfaces are increasingly isoenergetic with decreasing steric bulk (**G-G** > **V-V** ~ **T-T** > **I-I**).

Introduction

Conducting structure-activity relationships—a hallmark of small molecule drug design—relies on the assumption that modest changes in chemical composition will not significantly affect global conformation.[1] This belief allows molecular parameters to be rationally fine-tuned across bounded chemical space vis-à-vis the exploration of aliphatic groups to promote hydrophobic interactions. However, this assumption appears increasingly tenuous for macrocycles which contort between multiple

conformations of similar energy.[2-4] As a result, slight changes to composition can change the distribution of conformations as well as offer access to new conformation space.[5-7] Understanding and ultimately engineering conformation are of great interest as the community pursues the development of macrocyclic drugs.[8-12]

Through experiment and computation, strategies to understand, map, and control conformation space are emerging.[13-15] Studies survey existing collections[16,17] or known bioactive natural products.[18] Oftentimes the exploration centers on a single Murcko framework—a conserved arrangement of atoms—that is synthetically accessible or otherwise available.[19] Cyclic peptides attract significant attention in this regard.[20] Many of these frameworks are inspired by naturally bioactive molecules including Sanguinamide A[21] and somatostatin[22] or by observed bioactivity including the cyclic pentapeptides advanced by McAlpine.[23] In many cases, modest changes (e.g. methylation) can lead to a conformation change and an obfuscation of causality in a structure-activity relationship particularly with regard to passive cellular transport.

Assigning a molecular basis for causality requires knowledge of structure, itself a labor-intensive exercise. Employing a framework can facilitate these efforts, but still necessitates a determination of whether the change in composition constitutes a desired functional variation or leads to significant structural change. The development of predictive models that confirm conservation of molecular shape based on simple experiments—here, a 1D ^{1}H NMR spectrum and rOe pattern with a single resonance—can greatly accelerate these efforts.

Our longstanding interest in triazine chemistry[24] and recent studies of hydrazine-substituted triazines[25,26] led us to explore macrocycles incorporating triazinyl hydrazones as molecular frameworks.[27,28] The ease

of synthesis and the numerous sites available to explore functional variation make triazine-based macrocycles a versatile platform for pursuing structure-property relationships. Zerkowski and coworkers showed earlier that static, covalent chemistry could yield similar triazine targets.[29]

Initial efforts produced macrocycles ranging from 22-28 atoms—each a different Murcko framework—that displayed different molecular shapes ranging from ones that were compact and folded to those that were extended and flat.[27,28] During the course of these studies, however, two isomeric 24-atom macrocycles were prepared—one with glycine and a three carbon acetal (-NH$\underline{CH_2}$CONH$\underline{CH_2}\underline{CH_2}$C=N-) and the other with β-alanine and a two carbon acetal (-NH$\underline{CH_2}\underline{CH_2}$CONH$\underline{CH_2}$C=N-).[27] Both showed markedly similar, folded structures in the solid-state. To better define the conformational landscape associated with this framework, we chose to prepare additional 24-atom macrocycles that varied in the choice of amino acid. Incorporating β-branched amino acids—valine, threonine and isoleucine—offers the opportunity to probe steric tolerances. Chart 1 shows these targets as well as the labeling strategy that is adopted for the NMR spectra. These macrocycles are named for the amino acid of interest; **G-G**, **V-V**, **T-T** and **I-I.**

Chart 1. The Murcko framework, G-G and the β–branched macrocycles. The labels associated with the NMR spectra are provided. When the dimethylamine groups (with methyls M1 and M2) are replaced with morpholine groups, an apostrophe is appended to the name. Distances D1 and D2 are the collective variables used in the well-tempered metadynamics calculations. The isomers of **I-I** result from racemization of the α–stereocenter.

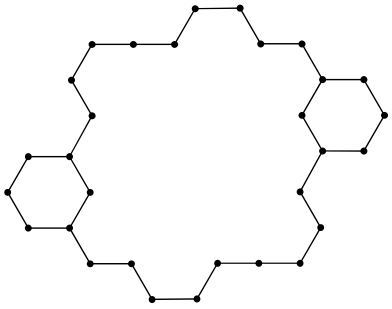

Framework

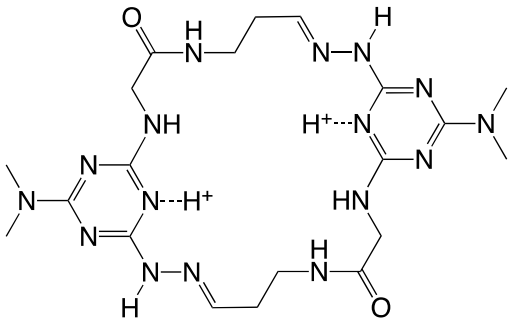

G - G

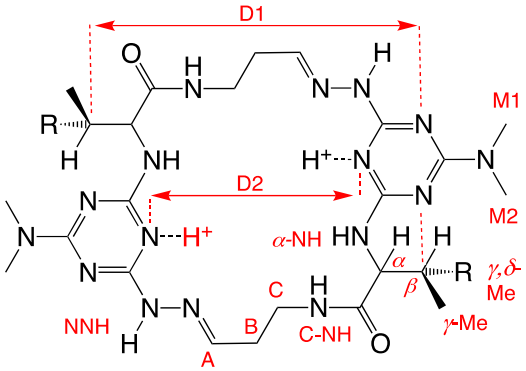

V - V
R = Me

T - T
R = OH

I - I
R = Et

Here, we establish that **G-G**, **V-V** and the isomers of **I-I** adopt a common 3-dimensional shape in solution and in the solid-state using NMR spectroscopy and x-ray crystallography, respectively. Structural assignment of **T-T** rests solely on NMR spectroscopy because no diffraction-quality crystals of **T-T** have been obtained. Trends in the NMR data reveal that structural predictions are possible and lead to a nuanced model for conformation. This model was applied successfully to both isomers of **I-I** before x-ray

structural data became available to reveal their relationship: they result from racemization of the α–stereocenter leading to an (S,S)-homodimer and an (R,S)-homodimer.

Experimental

*NMR Spectroscopy***.** Room temperature 1D ^{1}H NMR and ^{13}C{^{1}H} NMR spectra were recorded on a 400 MHz Bruker Avance spectrometer at Texas Christian University. Chemical shifts were referenced to the corresponding solvent resonance (e.g. DMSO-d_6, δ = 2.52 ppm). Low temperature spectra were acquired on a 500 MHz Varian NMR spectrometer at the University of North Texas in Denton. Structural assignments were made with additional information from COSY and HSQC experiments. Deuterated NMR solvents were used as purchased from either a bottle or ampule.

Well-tempered metadynamics simulations. The atomistic models were prepared using Antechamber,[30] parameterizing the bonded and non-bonded interactions following the Generalized Amber Force Field (GAFF). Atomic point charges were computed using the RESP approach[31] with HF/(6-31)G* theory by Gaussian 16.[32] After an initial minimization and equilibration, a 500 ns long well-tempered metadynamics (WT-MetaD)[33] simulation was run for each macrocycle with D1 and D2 as collective variables using Gromacs 2021.2[34] patched with Plumed.[35] After reaching convergence, the deposited bias was reweighted using the Tiwary-Parrinello free energy estimator to obtain the free energy surface.[36]

Crystallography. Diffraction data for CCDC 2221530 was collected at Texas Christian University at 100 K on a Bruker D8Quest Diffractometer. Diffraction data for CCDC 2233277 was collected at Texas A&M University. Data collection, frame integration, data reduction (multi-scan) and structure determination were carried out using APEX2 software.[37] Initial structural refinements were performed with XSHELL (v 6.3.1) by the full-matrix least-squares method.[38] All non-hydrogen atoms were refined using anisotropic

thermal parameters, while the hydrogen atoms were treated as mixed. OLEX2 was used for additional structure refinement and graphical representation.[39] Crystals suitable for x-ray diffraction were obtained by dissolving 50 mgs of macrocycle in 3 mL of methanol in a dram vial. The cap was loosely placed on top and the solvent was allowed to evaporate over two weeks. Crystals were obtained from the resulting residue.

General Chemistry and synthesis. Details of the synthesis and characterization of the macrocycles and intermediates appear in the supporting information.

Results and Discussion

Organization of this report. After introducing details of the synthesis, the focus shifts to the structural elements that define the conformation of this molecular framework**.** Common characteristics emerge including 1) the efficiency of macrocyclization, 2) common NMR features, 3) C2-symmetry, 4) an (E)-hydrazone, 5) a common site of protonation, 5) a conserved rotamer state, and 6) folded structures in solution and in the solid-state. From these criteria, a model to predict 3-dimensional structure is introduced. Subsequently, distinctive elements of this model that define subpopulations are advanced to identify subpopulations that vary subtly in conformation. Macrocycle **G-G** is different from **V-V** and the isomers of **I-I**. Macrocycle **T-T** shares elements of both groups. A computational analysis of the free energy surfaces is reported.

Synthesis and nomenclature. The details of the synthetic methods and its execution are described in the supporting information. Scheme 1 outlines the route employed. It represents an improvement over those previously published because it requires fewer synthetic steps and only one or two chromatographic separations.[27-28] Briefly, cyanuric chloride is substituted in a stepwise manner in a single reaction flask to

yield an acid intermediate named for the amino acid (e.g. **G-acid**). This protocol is used to install either the dimethylamine or morpholine auxiliary groups, the former more useful for NMR analysis and the latter more amenable to crystallization. After isolation and characterization, the acid is elaborated to the monomer (e.g. **G**). Treatment of the monomer with trifluoroacetic acid in dichloromethane followed by slow evaporation of the solvent quantitatively yields the macrocycle (e.g. **G-G**).

Scheme 1 Synthesis of the macrocycles. a) $BOCNHNH_2$, NaOH *(aq)*, THF, -10 °C, 0.5 h. b) Amino acid, NaOH *(aq)*, RT, 6 h. c) 40% $HN(CH_3)_2$ *(aq),* RT, 6 h. d) EDC-HCl, $H_2NCH_2CH_2CH(OCH_2CH_3)_2$, DIPEA, RT, DCM, 8 h. e) 1:1 DCM:TFA, 72 h.

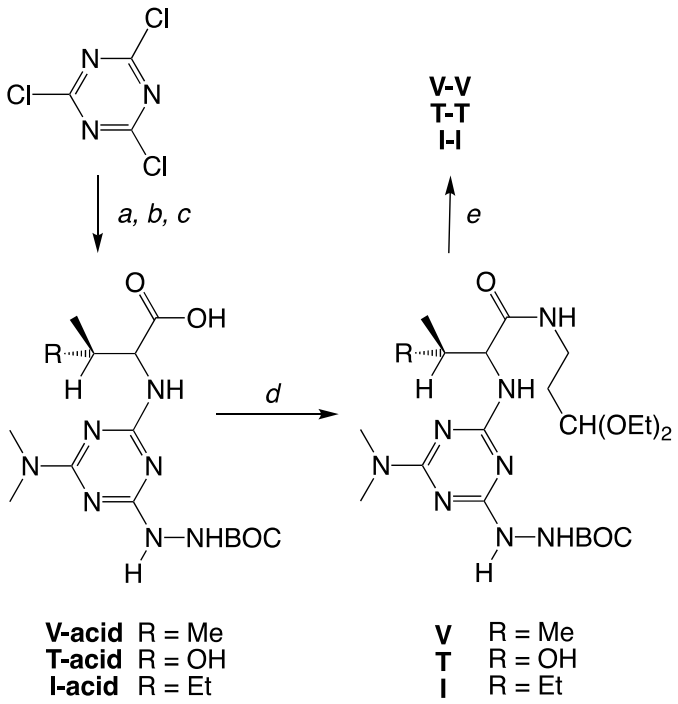

NMR spectroscopy provides the clearest evidence of macrocycle formation. Figure 1 shows the evolution of spectral complexity during the synthesis of **V-V**. The wealth of resonances for **V-acid** and acetal **V** derive from the existence of up to four rotamers resulting primarily from hindered rotation about the triazine-*N* bonds. The α-H of valine (labeled α) appears as three broad resonances between 4.5-4 ppm in **V-acid** in populations that are different than those of **V.** In macrocycle **V-V**, a single, resolved α-H is observed.

Similar patterns are seen in the region between 7-9 ppm of the intermediates wherein multiple signals for exchangeable protons are observed in **V-acid** and **V**. Single resonances are observed for NNH, C-NH and α-NH in the spectrum of **V-V**.

Figure 1. The 400 MHz ^{1}H NMR spectra of **V-acid**, **V** and **V-V** in DMSO-d_6 reveal convergence to a single species upon macrocyclization.

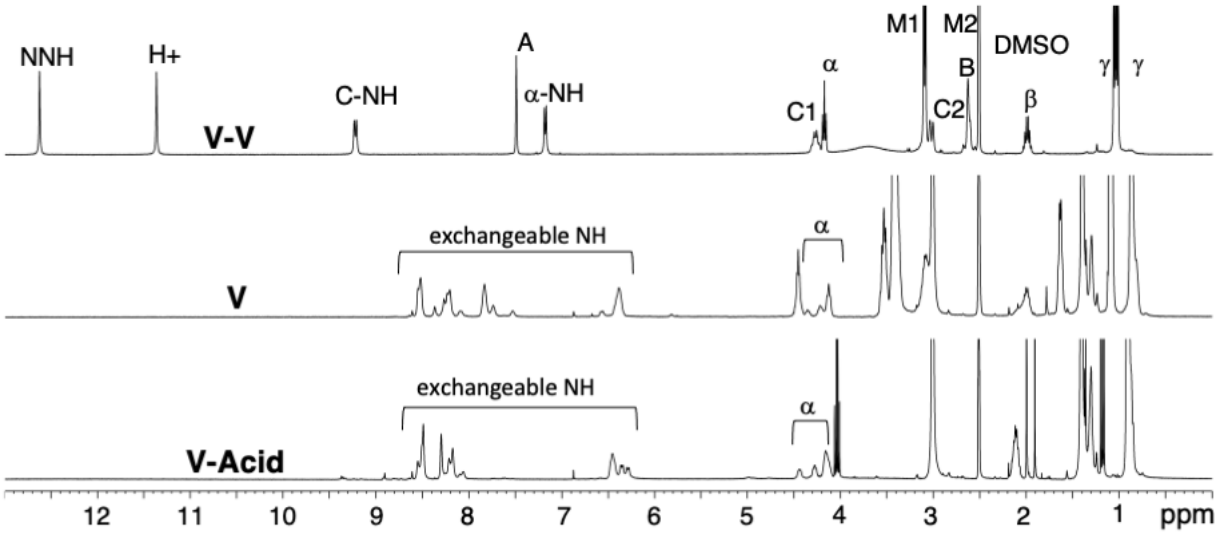

Characteristics common to the molecular framework. All of the macrocycles share seven characteristics. *Characteristic 1: Efficiency of macrocyclization.* These macrocycles are products of dynamic covalent synthesis, a method that is often plagued by yielding a diversity of products including oligomers and polymers that result from kinetic traps.[40] Here, the quantitative formation of macrocycles—independent of steric bulk—is surprising. We infer that these macrocycles represent thermodynamic minima and hypothesize that the acidic environment might template dimerization. Macrocyclization appears to be independent of concentration across the range explored to date—from 3 mM to 100 mM (corresponding to 5 mg/mL to 165 mg/mL). The rate of evaporation is critical to success. Slow evaporation of solvent with

stirring over 3-7 days provides the best results. Efforts to accelerate macrocyclization are ongoing. Accelerating the rate of evaporation by vacuum or air stream results in a mixture of species that we attribute to the aforementioned, kinetically-trapped side products which can be converted to macrocycle by addition of more acid and solvent. The effect of temperature, pH, or cosolvent choice on cyclization rates and/or product distributions have not been observed nor rigorously explored. These effects have been noted in other systems.[41] Such studies will be pursued in due course.

Characteristic 2: Common NMR features. Given its simplicity, the fingerprint region of the ^{1}H NMR between 7-13 ppm is particularly valuable for comparing different macrocycles. Figure 2 shows this region for **G-G**, **V-V**, **T-T**, and **I-I** in DMSO-d_6, a solvent that provides sharp resonances for the exchangeable protons. With the exception of α-NH, the general order of appearance of resonances is conserved: moving upfield the sequence is NNH, H+, C-NH, then A (N=C<u>H</u>). The categorization of these protons by color (yellow, blue and green) is addressed later.

Figure 2. The fingerprint region of the 400 MHz ^{1}H NMR spectra of **G-G**, **V-V**, **T-T**, and **I-I** in DMSO-d_6 shows well-resolved resonances and the appearance of two isomers for **I-I**. The arrow indicates the position of α-NH for **T-T**. The colored domains indicate subpopulations, **G-G**-like (yellow), **V-V**-like (blue), and intermediate (green).

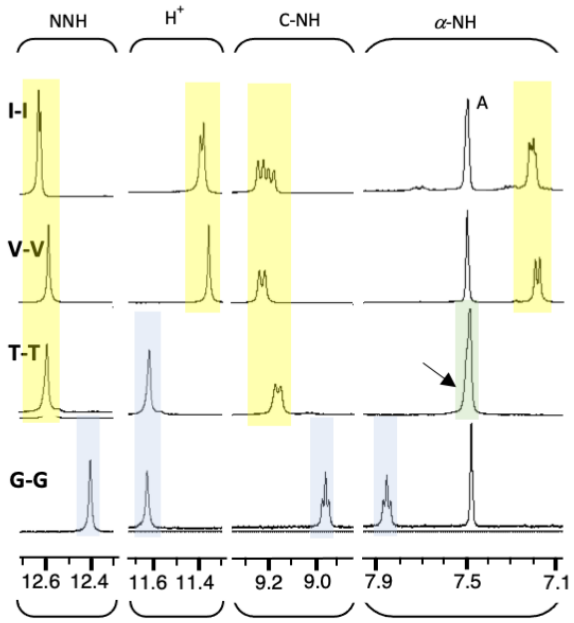

Characteristic 3: C2-symmetry in solution. The degeneracy observed in the ^{1}H NMR spectra—as shown in Figure 2 and in the upfield region as well—requires that both subunits of each macrocycle adopt C2-symmetric conformations, including both isomers of **I-I**.

The ^{13}C NMR spectra also reflect the symmetry of these macrocycles. Each spectrum presents a single set of degenerate resonances (Figure 3). Again, two resonances with unequal intensities are observed for **I-I**. These resonances are most evident for the carbonyl (173 ppm) and consistent with a mixture of two isomers, not a single asymmetric molecule.

Figure 3. The downfield region of the 100 MHz ^{13}C{^{1}H} NMR spectrum. Trifluoroacetic acid is present in the spectra (*q*, 159 ppm). The colored domains indicate subpopulations, **G-G**-like (yellow), **V-V**-like (blue), and intermediate (green).

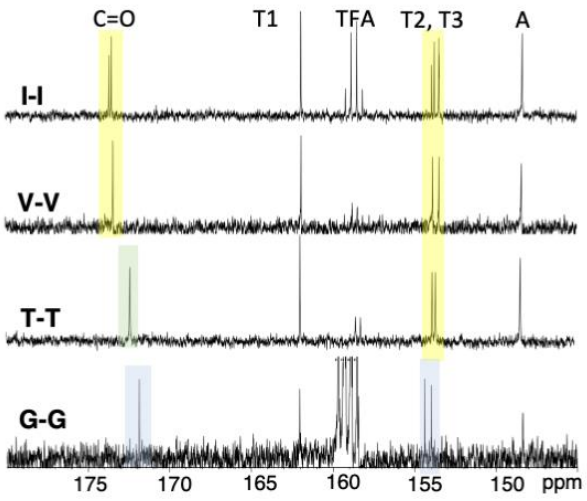

Characteristic 4: An (E)-hydrazone. More amenable to rOesy than nOesy experiments, the macrocycles show a strong correlation between A and NNH (Chart 2). Indeed, it is the most dominant signal in most cases. Cross peaks indicative of the (Z)-isomer are not observed across a variety of solvents (D_2O, CD_3CN, CD_3OD). Consistent with this observation, the crystal structures of the morpholine derivatives, **G'-G'**, **V'-V'**, and **I'-I'** adopt (E)-hydrazones.

Characterisic 5: A common site for protonation. The site of protonation can be determined by rOesy experiments. An rOe between H^+ and α-NH place these protons in close proximity. The absence of an rOe correlation between H^+ and either methyl group of the dimethylamine substituent, M1 or M2, argues for the proton on the opposite end of the triazine (Chart 2). The crystal structures of the morpholine derivatives **G'-G'**, **V'-V'**, and **I'-I'**, show protonation at this site. Intuition suggests that this site is preferred because the lone pair of the hydrazone -C=NNH- can offer additional electron density to stabilize protonation.

Chart 2. Site of protonation and the rotamers derived from hindered rotation about the triazine-*N* bond. Protonation occurs opposite the dimethylamine group and adjacent to α-NH. ROESY correlations observed (solid arrow) and absent (dotted arrow) confirm rotamer I is adopted in solution. Rotamer I is observed in the solid state.

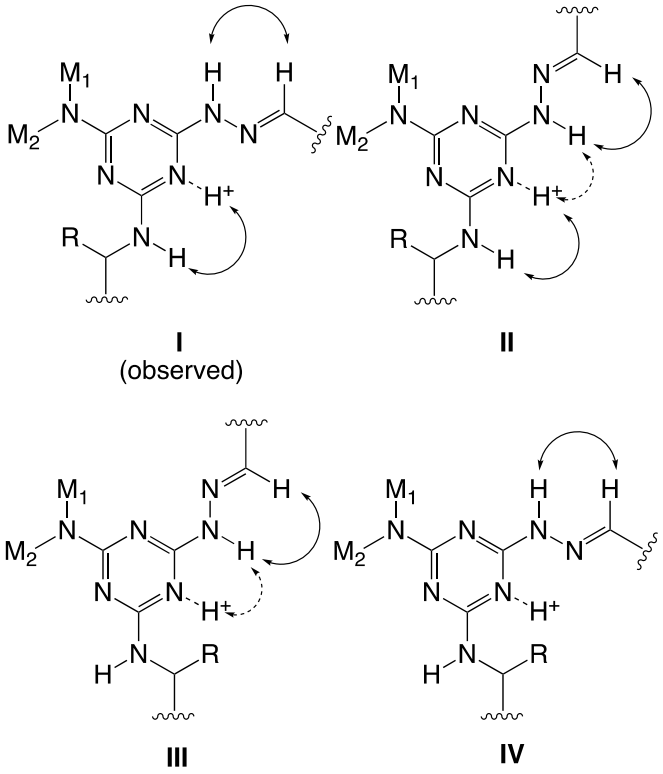

Characteristic 6: A common rotamer state. Hindered rotation about the triazine-*N* bonds lead to conformational isomers that are apparent in the acyclic intermediates.[41-46] The barrier to rotation for this bond in acyclic systems has been determined to be ~15 kcal/mol.[45] The macrocycles adopt a single rotamer state that can be assigned by rOesy experiments. The solid arrows in Chart 2 represent rOe correlations that are observed experimentally. The dotted arrows indicate ones that would be expected for the rotamer, but are not observed. Only rotamer I satisfies the experimental observations. That is, strong rOe correlations are observed between H^+ and α-NH, but not between H^+ and the NNH of the hydrazone. Rotamer I is also observed in the crystal structures of the morpholine derivatives, **G'-G'**, **V'-V'**, and **I'-I'.**

Characteristic 7: Folded conformations in solution and the solid-state. In solution, the macrocycles present an rOe between the hydrazone, A, and one or both of the auxiliary methyl groups, M1 and M2. Macrocycle **G-G** shows an rOe between A and both M1 and M2, while the β-branched macrocycles show only an rOe between A and M2. These correlations are shown in the supporting information (Figure S68). The distance between these groups requires that the molecule adopt a folded conformation as observed in the solid state.

The emergence of a predictive model. The ^{1}H and ^{13}C NMR data form the foundation of a model that is predictive of the conformational features of the framework (Table 1). Five resonances in the ^{1}H NMR and the network of rOes to A (to NNH to establish the (E)-hydrazone and to M1 to establish folding) convey critical structural information quickly. The carbonyl and A resonances in the ^{13}C NMR are of lesser importance, but also corroborate assignment.

Table 1. Comparison of features of the two structural models. The cells are colored to indicate **G-G**-like behavior (blue), **V-V**-like behavior (yellow), intermediate behavior (green) and common behavior (no color).

Characteristic	**G-G**	**T-T**	**V-V**	**I-I** (major)	**I-I** (minor)
δ ^{1}H NNH (ppm)	12.41	12.58	12.62	12.62	12.61
δ ^{1}H H+ (ppm)	11.63	11.62	11.36	11.39	11.37
δ ^{1}H C-NH (ppm)	8.94	9.16	9.22	9.23	9.18
δ ^{1}H A (ppm)	7.47	7.47	7.49	7.48	7.49
δ ^{1}H α-NH (ppm)	7.84	7.47	7.18	7.21	7.19
rOe A to NNH	strong	strong	strong	strong	strong
rOe A to M1 and M2	present	-	-	-	-
rOe A to M2 only	-	present	present	present	present
δ ^{13}C C=O (ppm)	171.4	171.9	172.9	173.0	173.2
δ ^{13}C A (ppm)	147.9	147.9	148.0	147.9	147.9

Subpopulation distinctions. Trends within the data suggest that even more nuanced elements of conformation can be inferred. Two subpopulations emerge as indicated by the colored domains of Table 1 (and Figures 2 & 3). One subpopulation is represented by **G-G**, the other subpopulation by **V-V** and the isomers of **I-I**. Macrocycle **T-T** shares elements of both. These distinguishing characteristics, so-called distinctions, arise from differences in *1)* $\pi-\pi$ stacking informed by the rOesy network, *2)* the dynamic behavior informed by variable temperature NMR experiments, and the diagnostic chemical shifts of *3)* NNH, *4)* C-NH, and *5)* α-NH.

Distinction 1: $\pi-\pi$ Stacking. To obtain crystals suitable for x-ray diffraction, dimethylamine was replaced with morpholine (leading to a shift in nomenclature from **G-G** to **G'-G'**, etc) because these derivatives are more amenable to crystallization[26-28] and behave like the dimethylamine analogues in solution. That is, all adopt an (E)-hydrazone, show identical protonation sites, common NMR features, the same rotamer states, and folded structures. Probing solution structure with morpholine derivatives using ^{1}H NMR spectroscopy is less desirable than using **G-G, V-V**, **T-T** and **I-I** because the axial and equatorial protons of the morpholine ring are not degenerate and crowd the spectrum between 4 ppm and 3 ppm whereas the methyl groups of dimethylamine appear as well-resolved singlets in an uncrowded region of the spectrum.

Figure 4 shows the crystal structures of **G'-G'**, **V'-V'** and the isomers of **I'-I'**. In the folded conformation, the substituents on the α-C of the amino acid are oriented into axial and equatorial positions. In these crystal structures, the α-H occupies the axial position and the sidechain occupies the equatorial position. For **G'-G'**, equatorial protons do not interact and the triazine rings do not stack upon each other. Instead, each triazine ring stacks on the hydrazone. In **V'-V'** and **I'-I'**, however, the sidechains do interact (presumably productively) leading to a translation of the π-system from **G-G** wherein $\pi-\pi$ stacking results in greater overlap of the triazine rings. The likely origins of the isomerism in **I'-I'** (and **I-I**) are revealed in

the crystal structure which contains two macrocycles in a unit cell (CCDC 2221530). One macrocycle comprises isoleucine residues that preserve the stereochemistry (S,S). The other macrocycle derives from allothreonine (R,S) resulting from epimerization of the a-carbon under the conditions of the synthesis. An additional crystal structure comprising just the (S,S) isomer has also been solved (CCDC 2233277).

Figure 4. The crystal structures of an morpholine analogues **G'-G'**, **V'-V'** and the two isomers of **I'-I'** from the top and edge. The labels A, M1 and M2 correspond to specific hydrogen atoms that establish folding as well as subpopulation. The labels "a" and "e" correspond to axial and equatorial positions within the macrocycle. The isomers of **I'-I'** derive from epimerization of the α-carbon.

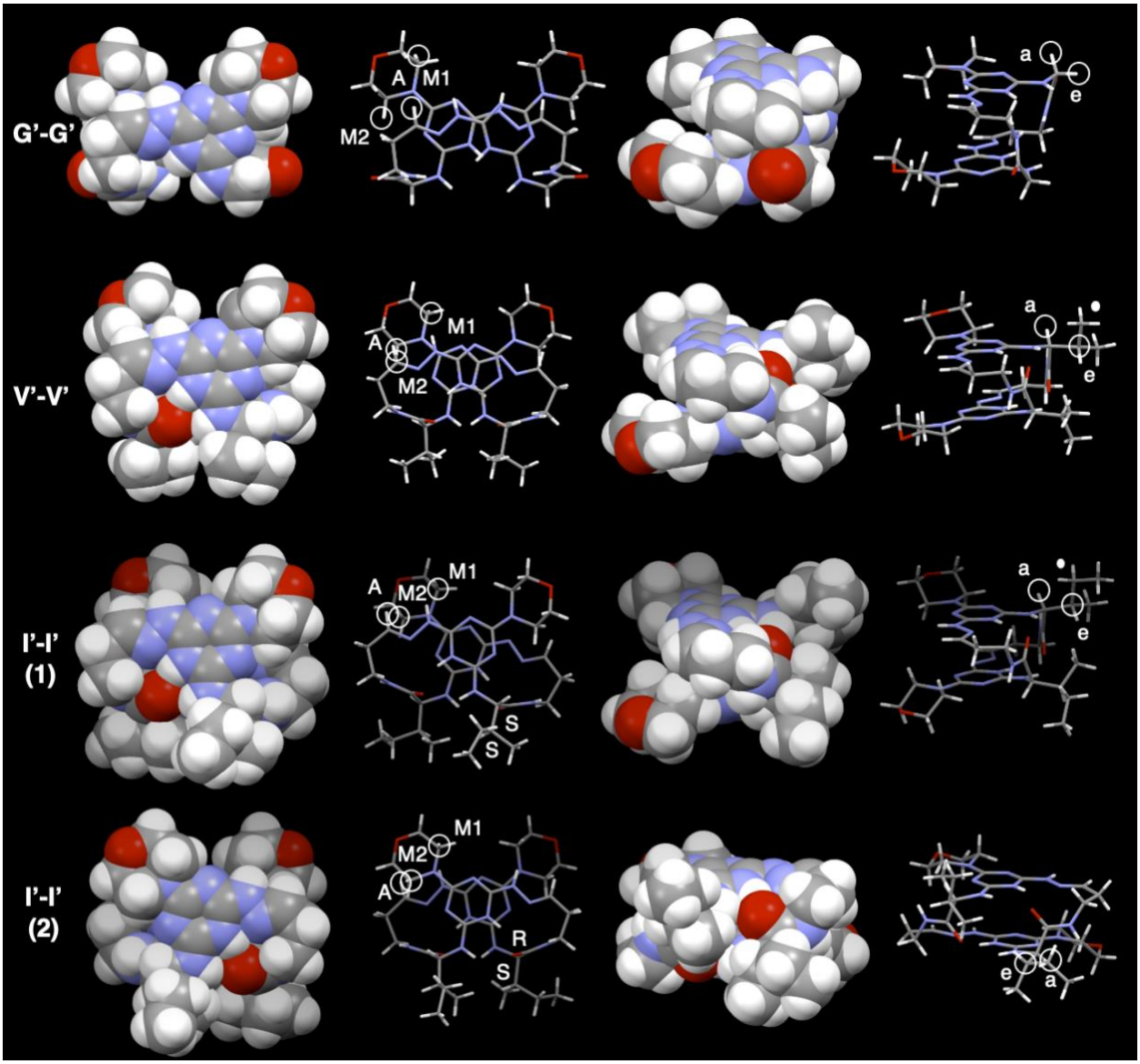

This difference in stacking is reflected in rOesy data: the rOe network of **G-G** differs from that of the β-branched macrocycles. Both populations show a strong rOe between A and NNH, establishing the (E)-hydrazone. However, the evidence for a folded structure is distinct. Macrocycle **G-G** shows rOes to M1 and M2. The β-branched macrocycles only show an rOe to M2. The crystal structures offer a compelling interpretation of this data. In the solid state, the $\pi-\pi$ stacking of triazine-on-hydrazone in **G'-G'** places proton A between M1 and M2 (circled in Figure 4). In **V'-V'** and the isomers of **I'-I'** however, triazine-on-

triazine overlap is more substantial, leading to an increased distance between proton A and M1 precluding this rOe, but conserving the rOe between A and M2. It is noteworthy that the rOe observed between A and M2 is stronger for the major isomer than the minor isomer, but crystal structure data is not compelling enough to justify a tentative assignment of these isomers.

Distinction 2: The chemical shift of H^+. The chemical shift of H^+ differs across the subpopulations, appearing at 11.6 ppm for **G-G** and ~11.4 ppm for **V-V** and both isomers of **I-I**. While the source of the difference remains unclear, two hypotheses are noteworthy. The first hypothesis rests on the crystal structure data: the π–system might influence the chemical shift of H^+ because it appears positioned within the ring current of the triazine for **V'-V'** and **I'-I'**, but more distant for **G'-G'**. The second (and favored) hypothesis rests on differences in dynamic motion that modulate the availability of the carbonyl to engage in hydrogen bonding. In the crystal structure of **G'-G'**, the carbonyl points outwards towards solvating molecules bridging unit cells while the carbonyls of **V'-V'** and the isomers of **I'-I'** points inward to engage in hydrogen bonding with H^+. With the recognition that crystal packing forces can influence conformation, the upfield shift of H^+ for **V-V** and the isomers of **I-I** is consistent with increased electron density for H^+.

In addition, variable temperature NMR experiments reveal markedly different behavior amongst this series of macrocycles. We have reported that **G-G** moves between two folded, enantiomeric states[47] by way of an extended structure.[48] Importantly, these two states interconvert the axial and equatorial positions of the both α-H and the C protons much like the ring-flip in cyclohexane. Accordingly, at high temperatures, a single resonance is observed. At lower temperatures, this resonance decoalesces to reveal both the axial and equatorial positions. Neither coalescence or decoalescence has been observed across the available temperature range for the β-branched macrocycles leading us to posit that this

motion is limited in these molecules, and accordingly, the hydrogen bond between H^+ and the carbonyl is more faithfully maintained.

Variable temperature (VT) NMR provides an additional distinction between these subpopulations. Protons involved in structure vis-à-vis hydrogen-bonding are less sensitive to temperature changes than those that are solvent accessible.[49] For proteins, a VT coefficient that is more negative than -4.5 ppb/degree for an amide-NH conveys that it is exposed to solvent and not engaged in structure. Values more positive than -4.5 ppb/degree convey that the amide is engaged in a hydrogen bond or that another structural feature shields it from solvent. In evaluating the VT coefficients for these macrocycles, we abandon this numeric benchmark and refrain from making comparisons across proton types. However, restricting the discussion to protons of the same type (e.g. NNH) has value and reveals interesting trends.

Table 2 shows that the VT coefficients across the macrocycles are distinct by subpopulation. It is apparent that **V-V**, **T-T** and **I-I** behave similarly and collectively different than **G-G**. This trend is consistent with the difference in the dynamic behavior reported. The exchangeable NHs yield the most consistent picture with NNH, C-NH and α-NH of **G-G** are more sensitive to temperature, and thus, less protected from solvent than those same protons of the β-branched macrocycles.

Table 2. Variable temperature coefficients (Δppb/ΔT) for exchangeable protons of the macrocycles reported in ppb. The areas shaded blue and yellow convey distinguishing characteristics of the subpopulations. Green indicates an intermediate value.

		G-G	T-T	V-V	I-I (maj)	I-I (min)
VT coeffi	NNH	-0.8	0.1	0.6	0.7	0.9
	H+	-2.0	-1.7	-1.7	-2.2	-2.2
	C-NH	-3.8	-1.8	-1.9	-2.0	-1.7

α-NH	-1.5	0.2	0.3	0.3	0.3
A	0.6	0.3	0.1	0.3	0.3
OH	-	0.7	-	-	

Distinction 3: Chemical shift of NNH. The subpopulations differ in the chemical shift of the NNH resonance in DMSO-d_6. It appears at 12.6 ppm for the β-branched macrocycles and at or 12.4 ppm for **G-G**. This difference might be attributed to the extent to which the hydrazone lone pair contributes to hydrogen bonding, the influence of the π-system, or a reflection of dynamic behavior and contributions of the carbonyl. While the molecular basis remains unknown, the chemical shift of NNH is a distinct signature of subpopulation.

Distinction 4: Chemical shift of C-NH. The subpopulations differ in the position of C-NH in DMSO-d_6 with **G-G** at 8.95 ppm and **V-V** and isomers of **I-I** at 9.35 ppm. We hypothesize that the downfield shift for the β-branched macrocycles is consistent with the carbonyl hydrogen bonding to H^+. Polarization of the carbonyl increases the π-character of the amide bond leading to a downfield shift of this amide NH for the β-branched macrocycles.

Distinction 5: Chemical shift of α-NH. The α-NH proton shows the most significant difference when considering the two subpopulations. In DMSO-d_6, it appears downfield at 8.9 ppm for **G-G**, but at 9.2 ppm for **V-V** and **I-I**. We infer that the α-NH σ-bond of **G-G** contributes electron density to H^+ to offset the diminished contributions of the carbonyl group.

The structure of T-T. Interestingly, **T-T** adopts elements of both subpopulations. Resonances for NNH and CNH align with **V-V** and the isomers of **I-I** as do the variable temperature coefficients reported. In contrast, the resonance for H+ aligns with **G-G**. The chemical shift of α-NH falls evenly between the two

subpopulations. The data suggests that **T-T** adopts a conformation most similar to **V-V** and the isomers of **I-I.** However, stabilization of H^+ by the carbonyl is significantly reduced—making **T-T** more like **G-G**. We hypothesize that electron density from the carbonyl is reduced at H+ by competitive hydrogen bonding between it and the β-hydroxyl group. The chemical shift of the β-OH resonance (5.48 ppm) is consistent with hydrogen bonding.

The free energy surfaces. To conclude these studies, we employed well-tempered metadynamics (WT-MetaD)[33] to probe the free energy landscape. Classical molecular dynamics calculations can suffer from entrapment in local energy minima[51,52] while WT-MetaD can sample configurations more than than 2kT higher in free energy. The two collective variables, D1 and D2 (Chart 1), were chosen to capture both extended and folded molecules. D1 is defined as the distance between the β-carbons of the β-branched amino acid or the α-proton of glycine. D2 is the distance between protonated nitrogens. These distances become the ordinates used to generate the free energy surface (FES) shown in Figure 6.

The regions on the left side of the FES plots (low D1) correspond to those structures with significant sidechain-sidechain interactions. Regions on the right are populated with structures that orient the sidechains distant from one another. Distances derived from the crystal structures are indicated with circles.

Figure 6. Free energy surfaces (left) and population plots (right) for the four macrocycles. Each contour of the FES corresponds to 1 kT. The circles reflect the data observed in the crystal structures. The relative populations of each minima are indicated. The population comprises all structures within 3 kT of the local minima corresponding to red and orange domains.

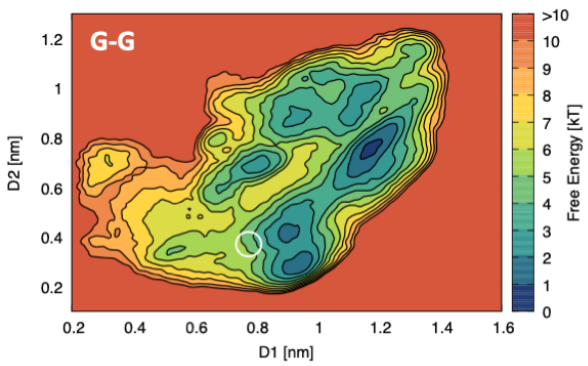
G-G
D2 [nm]
D1 [nm]
Free Energy [kT]
>10

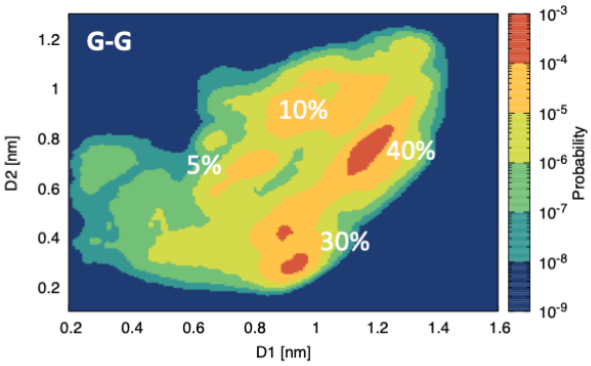
G-G
10%
40%
5%
30%
D2 [nm]
D1 [nm]
Probability

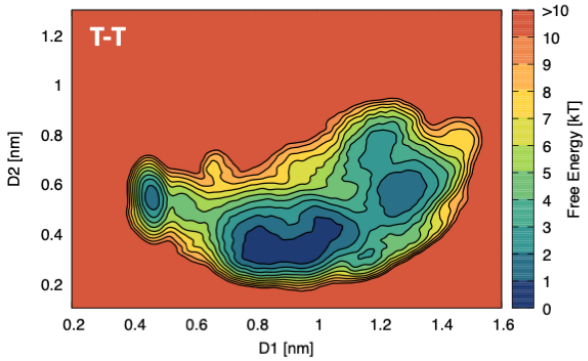
T-T
D2 [nm]
D1 [nm]
Free Energy [kT]
>10

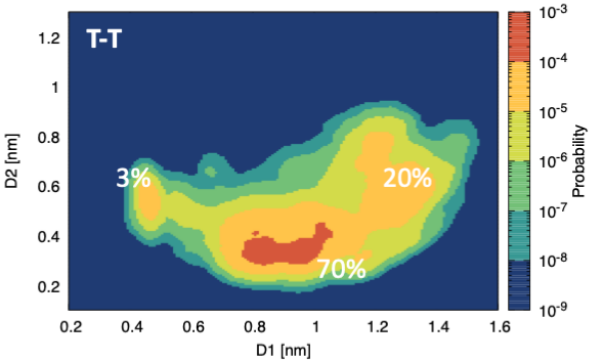
T-T
3%
20%
70%
D2 [nm]
D1 [nm]
Probability

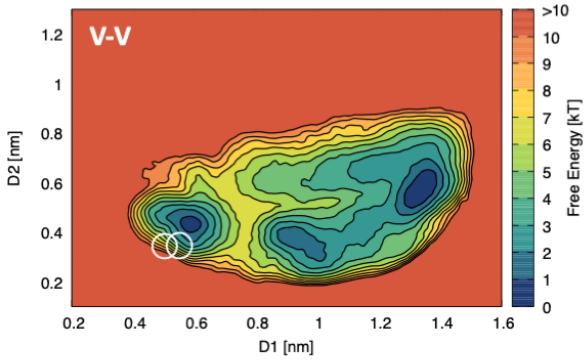
V-V
D2 [nm]
D1 [nm]
Free Energy [kT]
>10

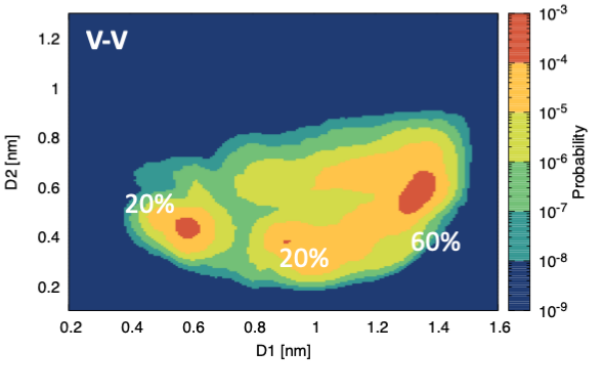
V-V
20%
20%
60%
D2 [nm]
D1 [nm]
Probability

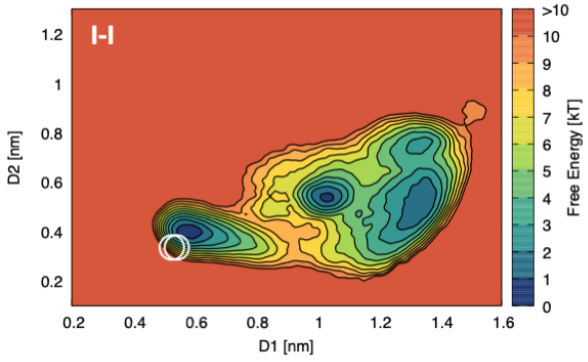
I-I
D2 [nm]
D1 [nm]
Free Energy [kT]
>10

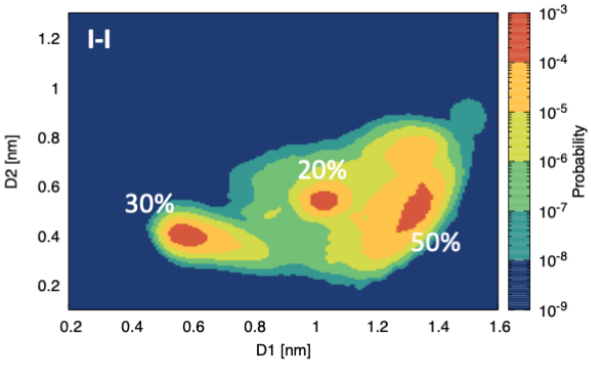
I-I
30%
20%
50%
D2 [nm]
D1 [nm]
Probability

The results are consistent with expectations: these macrocycles are flexible and can adopt many different conformations within a few kT of each other, a situation ideal for the design of molecular chameleons. The FES of **G-G** shows multiple shallow minima with regions between them populated with other structures of similar energy. In contrast, the FES of the β-branched macrocycles has three well-defined minima.

The FES also shows that increasing steric bulk reduces the size of the conformational footprint: **G-G** (4.1 nm^2) > **V-V** (2.9nm^2) ~ **T-T** (2.8 nm^2) > **I-I** (2.3 nm^2). In terms of percent differences relative to **G-G** (100%), the area of **V-V** is 69% of **G-G** while **T-T** at 68%. Both exceed that of **I-I** at 55%.

These FESs can be used to calculate the relative probabilities *P(r)* to determine populations of structures using equation 1.

$$P(r) \propto e^{-\frac{G(r)}{kT}} \qquad \text{(Eq. 1)}$$

These probability maps are shown in Figure 9 (right). The populations indicated are based on including structures within 3 kT of the minima (the red and orange domains of the FES). The shallow FES of **G-G** is reflected in the population (15%) that exists on the surface not defined by local minima. These populations cannot readily relate to specific structures observed in solution, only the D1 and D2 coordinates because each minimum is populated by a range of different structures ranging from those that are compact with significant π–π overlap to those that are more extended.

Conclusion

The data derived from solution and solid-state provides a clear picture of attributes conserved across this molecular framework. From a 1-D ^{1}H NMR spectrum and the measurements of rOe correlations with A, a nuanced determination of conformation can be obtained that allows assignment of specific subpopulations. Table 3 summarizes the spectroscopic features and the elements reported.

Table 3. Comparison of features of the two structural subpopulations of this molecular scaffold.

Characteristic	**V-V** subpop.	**G-G** Subpop.	**Reports on…**
δ^{1}H NNH (ppm)	12.62	12.41	NNH hydrogen bonding
δ^{1}H H+ (ppm)	11.36	11.63	C=O orientation/dynamics; π–π stacking
δ^{1}H C-NH (ppm)	9.22	8.94	C=O hydrogen bonding/dynamics
δ^{1}H A (ppm)	----------7.5----------		Macrocyclization
δ^{1}H α-NH (ppm)	7.2	7.47	Hydrogen bonding; π–π stacking
rOe A to NNH	----------strong----------		(E)-Hydrazone
rOe A to M1 & M2	-	present	Folding; π–π stacking of triazine-on-hydrazone
rOe A to M1 only	present	-	Folding; π–π stacking of triazine-on-triazine
δ ^{13}C C=O (ppm)	172.9	171.4	Hydrogen-bonding of CO to H+
δ ^{13}C A (ppm)	148.0	147.9	(E)-Hydrazone

The lessons learned have clear value as we consider strategies for drug design wherein small differences in shape can greatly influence physicochemical properties. Indeed, we propose that the 24-atom macrocycle represents a molecular framework amenable to substitution of the α-amino acid without loss of conformation. Functionalization at the α-carbon places groups more proximate than functionalization at the auxiliary positions of the triazine (e.g. replacing dimethylamine or morpholine). Additionally, the choice of glycine or the β-branched alternatives will influence the dynamic motion afforded the framework. Probing the generality of this model is currently in progress.

In addition, these studies contribute to a better understanding of these macrocycles which are "stable" in a descriptive sense. They can be stored at room temperature in organic solvents and acidic water

without signs of hydrolysis. They survive conventional silica gel chromatography. Ongoing efforts address the mechanistic basis for the quantitative cyclization (a result we hypothesize to be due to templating through the formation of a network of hydrogen bonds), the chiral sorting that appears to occurring and the reaction conditions required to minimize racemization.

Supporting Information & Data Availability. Synthetic methods, NMR spectra and crystallographic data (96 pp). All the data needed to reproduce our calculations can be found in the linked Github repository: https://github.com/GMPavanLab/Macrocycles2 (this link will be changed with its definitive zenodo URL upon acceptance).

Corresponding Authors

Riccardo Capelli – *Department of Biosciences, Università degli Studi di Milano, Via Celoria 26, 20133 Milan, Italy*; orchid.org/0000-0001-9522-3132; E-mail: riccardo.capelli@unimi.it

Eric E. Simanek – *Department of Chemistry & Biochemistry, Texas Christian University, Fort Worth, TX 76109, USA;* orcid.org/0000-0002-3195-4523; E-mail: e.simanek@tcu.edu

Authors

Alexander J. Menke – *Department of Chemistry & Biochemistry, Texas Christian University, Fort Worth TX 76129 USA*; orchid.org/0000-0001-9573-7045

Camryn J. Gloor – *Department of Chemistry & Biochemistry, Texas Christian University, Fort Worth TX 76129 USA*; orchid.org/0000-0001-9853-8017

Liam E. Claton – *Department of Chemistry & Biochemistry, Texas Christian University, Fort Worth TX 76129 USA*; orchid.org/0000-000204030-0281

Magy A. Mekhail – *Department of Chemistry & Biochemistry, Texas Christian University, Fort Worth TX 76129 USA*; orchid.org/0000-0001-5227-7114

Hongjun Pan – *Department of Chemistry, University of North Texas, Denton TX 76203 USA;* orchid.org/0000-0002-9230-8656

Mikaela D. Stewart – *Department of Biology, Texas Christian University, Fort Worth TX 76129 USA;* orchid.org/0000-0002-0809-9469

Kayla N. Green – *Department of Chemistry & Biochemistry, Texas Christian University, Fort Worth TX 76129 USA*; orchid.org/0000-0001-8816-7646

Joseph H. Reibenspies – *Department of Chemistry, Texas A&M University, College Station TX 77845 USA;* orchid.org/0000-0001-7595-5248

Giovanni M. Pavan – *Department of Innovative Technologies, University of Applied Sciences and Arts of Southern Switzerland, Polo Universitario Lugano, 6962 Lugano-Viganello, Switzerland and Department of Applied Science and Technology, Politecnico di Torino, 10129 Torino, Italy;* orchid.org/0000-0002-3473-8471

Author Contributions

AJM performed synthesis and supervised synthetic efforts of undergraduates CJG and LEC. MAM and JHR solved crystal structures. KNG and JHR supervised crystallographic studies. HP collected low temperature NMR data. MDS consulted on NMR techniques. GMP supervised computational analysis performed and analyzed RC. EES supervised the project. All authors contributed to writing the manuscript.

Notes

The authors declare no competing financial or conflicts of interest.

Acknowledgment

We thank the Robert A. Welch Foundation (EES A- P-0008-19730319; KNG P- 2063-20210327) and the NIH (EES R15GM135900; KNG 2R15GM123463). We also acknowledge preliminary efforts towards the preparation and characterization of these molecules by Jason Mars and Lucas Davison.

References

1. Bissantz, C.; Kuhn, B.; Stahl, M. A Medicinal Chemist's Guide to Molecular Interactions. *J. Med. Chem.* **2010**, 53, 5061-5084.

2. Ono, S.; Naylor, M. R.; Townsend, C. E.; Okumura, C.; Okada, O.; Lee, H. W.; Lokey, R. S. Cyclosporin A: Conformational Complexity and Chameleonicity. *J. Chem. Inf. Model.* **2021**, 61, 5601-5613.

3. Kamenik, A. S.; Lessel, U.; Fuchs, J. E.; Fox, T.; Liedl, K. R. Peptidic Macrocycles - Conformational Sampling and Thermodynamic Characterization. *J. Chem. Inf. Model.* **2018**, 58, 982-992.

4. Eastwood, J. R. B.; Jiang, L.; Bonneau, R.; Kirschenbaum, K.; Renfrew, P. D. Evaluating the Conformations and Dynamics of Peptoid Macrocycles. *J. Phys. Chem. B.* **2022**, 126, 5161-5174.

5. McTiernan, T. J.; Diaz, D. B.; Saunders, G. J.; Sprang, F.; Yudin, A. K. Navigating complex peptide structures using macrocycle conformational maps. *RSC Chem. Biol.* **2022**, 6, 739-747.

6. Sebastiano, M. R.; Doak, B. C.; Backlund, M.; Poongavanam, V.; Over, B.; Ermondi, G.; Caron, G.; Matsson, P.; Kihlberg, J. Impact of Dynamically Exposed Polarity on Permeability and Solubility of Chameleonic Drugs Beyond the Rule of 5. J. Med. Chem. **2018**, 61, 4189-4202.

7. Diaz, D. B.; Appavoo, S. D.; Bogdanchikova, A. F.; Lebedev, Y.; McTiernan, T. J.; dos Passos Gomes, G.; Yudin, A. K. Illuminating the dark conformational space of macrocycles using dominant rotors. *Nat. Chem.* **2021**, 13, 218-222.

8. Villar, E. A.; Beglov, D.; Chennamadhavuni, S.; Porco, J. A.; Kozakov, D.; Vajda, S.; Whitty, A. How proteins bind macrocycles. *Nat. Chem. Biol.* **2014**, 10, 723-731.

9. Dougherty, P. G.; Qian, Z. Q.; Pei, D. H. Macrocycles as protein-protein interaction inhibitors. *Biochem. J.* **2017**, 474, 1109-1125.

10. Tyagi, M.; Begnini, F.; Poongavanam, V.; Doak, B. C.; Kihlberg, J. Drug Syntheses Beyond the Rule of 5. *Chem. Eur. J.* **2020**, 26, 49-88.

11. Furukawa, A.; Schwochert, J.; Pye, C. R.; Asano, D.; Edmondson, Q. D.; Turmon, A. C.; Klein, V. G.; Ono, S.; Okada, O.; Lokey, R. S. Drug-Like Properties in Macrocycles above MW 1000: Backbone Rigidity versus Side-Chain Lipophilicity. *Angew. Chem. Int. Ed.* **2020**, 59, 21571-21577.

12. Vinogradov, A. A.; Yin, Y. Z.; Suga, H. Macrocyclic Peptides as Drug Candidates: Recent Progress and Remaining Challenges. *J. Am. Chem. Soc.* **2019**, 141, 4167-4181.

13. Hill, T. A.; Shepherd, N. E.; Diness, F.; Fairlie, D. P. Constraining Cyclic Peptides To Mimic Protein Structure Motifs. *Angew. Chem. Int. Ed*. **2014**, 53, 13020-13041.

14. Jwad, R.; Weissberger, D.; Hunter, L. Strategies for Fine-Tuning the Conformations of Cyclic Peptides. *Chem. Rev.* **2020**, 120, 9743-9789.

15. Appavoo, S. D.; Huh, S.; Diaz, D. B.; Yudin, A. K. Conformational Control of Macrocycles by Remote Structural Modification. *Chem. Rev.* **2019**, *119*, 9724-9752.

16. Rzepiela, A. A.; Viarengo-Baker, L. A.; Tatarskii, V.; Kombarov, R.; Whitty, A. Conformational Effects on the Passive Membrane Permeability of Synthetic Macrocycles. *J .Med. Chem.* **2022**, 65, 10300–10317.

17. Over, B.; Matsson, P.; Tyrchan, C.; Artursson, P.; Doak, B. C.; Foley, M. A.; Hilgendorf, C.; Johnston, S. E.; Lee, M. D.; Lewis, R. J.; McCarren, P.; Muncipinto, G.; Norinder, U.; Perry, M. W. D.; Duvall, J. R.; Kihlberg, J. Structural and conformational determinants of macrocycle cell permeability. *Nat. Chem. Biol.* **2016**, 12, 1065-1074.

18. Danelius, E.; Poongavanam, V.; Peintner, S.; Wieske, L. H. E.; Erdelyi, M.; Kihlberg, J. Solution Conformations Explain the Chameleonic Behaviour of Macrocyclic Drugs. *Chem. Eur. J.* **2020**, 26, 5231-5244.

19. Bemis, G. W.; Murcko, M. A. The Properties of Known Drugs. 1. Molecular Frameworks. *J. Med. Chem.* **1996**, 39, 2887-2893.

20. Buckton, L. K.; Rahimi, M. N.; McAlpine, S. R. Cyclic Peptides as Drugs for Intracellular Targets: The Next Frontier in Peptide Therapeutic Development. *Chem. Eur. J.* **2021**, 27, 1487-1513.

21. Bockus, A. T.; Schowchert, J. A.; Pye, C. R.; Townsend, C. E.; Sok, V.; Bednarek, M. A.; Lokey, R. S. Going out on a limp: dilineating the effects of branching, N-methylation and side chain size on the

passive permeability, solubility and fleixibility of Sanguinamide A analogs. *J. Med. Chem.* **2015**, 58, 4581-4589.

22. Biron, E.; Chatterjee, J.; Ovadia, O.; Langenegger, D.; Brueggen,J.; Hoyer, D.; Schmid, H. A.; Jelinek, R.; Gilon, C.; Hoffman, A.; Kessler, H. Improving Oral Bioavailability of Peptides by Multiple N-Methylation: Somatostatin Analogues. *Angew. Chem. Int. Ed.* **2008**,47,2595–259

23. Buckton, L. K.; McAlpine, S. R. Improving the Cell Permeability of Polar Cyclic Peptides by Replacing Residues with Alkylated Amino Acids, Asparagines, and D-Amino Acids *Org. Lett.* **2018**, 20, 3, 506–509.

24. Simanek, E. E. Two Decades of Triazine Dendrimers. *Molecules* **2021**, *26*(16), 4774.

25. Yepremyan, A.; Mehmood, A.; Brewer, S. M.; Barnett, M. M.; Janesko, B. G.; Akkaraju, G.; Simanek, E. E.; Green, K. N. A new triazine bearing a pyrazolone group capable of copper, nickel, and zinc chelation. *RSC Adv.* **2018**, 8, 3024-3035.

26. Ji, K.; Lee, C.; Janesko, B. G.; Simanek, E. E. Triazine-Substituted and Acyl Hydrazones: Experiment and Computation Reveal a Stability Inversion at Low pH. *Mol. Pharm.* **2015**, 12, 2924-2927.

27. Sharma, V. R.; Mehmood, A.; Janesko, B. G.; Simanek, E. E. Efficient syntheses of macrocycles ranging from 22-28 atoms through spontaneous dimerization to yield bis-hydrazones. *RSC Adv.* **2020**, 10, 3217-3220.

28. Yepremyan, A.; Mehmood, A.; Asgari, P.; Janesko, B. G.; Simanek, E. E. Synthesis of Macrocycles Derived from Substituted Triazines. *Chembiochem* **2019**, 20, 241-246.

29. Zerkowski, J. A.; Hensley, L. M.; Abramowitz, D. Triazinyl-amino acids, new building blocks for pseudopeptides. *Synlett* **2002**, (4), 557-560.

30. Case, D. A.; Aktulga, H. M.; Belfon, K.; Ben-Shalom, I. Y.; Brozell, S. R.; Cerutti, D. S.; Cheatham, III, T. E.; Cisneros, G. A.; Cruzeiro, V. W. D.; Darden, T. A.; Duke, R. E.; Giambasu, G.; Gilson, M. K.; Gohlke, H.; Goetz, A. W.; Harris, R.; Izadi, S.; Izmailov, S. A.; Jin, C.; Kasavajhala, K.; Kaymak, M. C.; King, E.; Kovalenko, A.; Kurtzman, T.; Lee, T. S.; LeGrand, S.; Li, P.; Lin, C.; Liu, J.; Luchko, T.; Luo, R.; Machado, M.; Man, V.; Manathunga, M.; Merz, K. M.; Miao, Y.; Mikhailovskii, O.; Monard, G.; Nguyen, H.; O'Hearn, K. A.; Onufriev, A.; Pan, F.; Pantano, S.; Qi, R.; Rahnamoun, A.; Roe, D. R.; Roitberg, A.; Sagui, C.; Schott-Verdugo, S.; Shen, J.; Simmerling, C. L.; Skrynnikov, N. R.; Smith, J. Swails, J.; Walker, R. C.; Wang, J.; Wei, H.; Wolf, R. M.; Wu, X.; Xue, Y.; York, D. M.; Zhao, S.; Kollman, P. A. (2021), Amber 2021, University of California, San Francisco.

31. Bayly, C. I.; Cieplak, P.; Cornell, W. D.; Kollman, P. A. A well-behaved electrostatic potential based method using charge restraints for deriving atomic charges – the RESP model. *J. Phys. Chem.* **1993**, 97, 10269-10280.

32. Gaussian 16, Revision C.01, Frisch, M. J.; Trucks, G. W.; Schlegel, H. B.; Scuseria, G. E.; Robb, M. A.; Cheeseman, J. R.; Scalmani, G.; Barone, V.; Petersson, G. A.; Nakatsuji, H.; Li, X.; Caricato, M.; Marenich, A. V.; Bloino, J.; Janesko, B. G.; Gomperts, R.; Mennucci, B.; Hratchian, H. P.; Ortiz, J. V.; Izmaylov, A. F.; Sonnenberg, J. L.; Williams-Young, D.; Ding, F.; Lipparini, F.; Egidi, F.; Goings, J.; Peng, B.; Petrone, A.; Henderson, T.; Ranasinghe, D.; Zakrzewski, V. G.; Gao, J.; Rega, N.; Zheng, G.; Liang, W.; Hada, M.; Ehara, M.; Toyota, K.; Fukuda, R.; Hasegawa, J.; Ishida, M.; Nakajima, T.; Honda, Y.; Kitao, O.; Nakai, H.; Vreven,

T.; Throssell, K.; Montgomery, J. A., Jr.; Peralta, J. E.; Ogliaro, F.; Bearpark, M. J.; Heyd, J. J.; Brothers, E. N.; Kudin, K. N.; Staroverov, V. N.; Keith, T. A.; Kobayashi, R.; Normand, J.; Raghavachari, K.; Rendell, A. P.; Burant, J. C.; Iyengar, S. S.; Tomasi, J.; Cossi, M.; Millam, J. M.; Klene, M.; Adamo, C.; Cammi, R.; Ochterski, J. W.; Martin, R. L.; Morokuma, K.; Farkas, O.; Foresman, J. B.; Fox, D. J. Gaussian, Inc., Wallingford CT, 2016.

33. Barducci, A.; Bussi, G.; Parrinello, M. Well-tempered metadynamics: A smoothly converging and tunable free-energy method. **Phys. Rev. Lett. 2008**, 100, 020603.

34. Abraham, M. J.; Murtola, T.; Schulz, R.; Pall, S.; Smith, J. C.; Hess, B.; Lindahl, E. Gromacs: High Performance Molecular Simulations through Multi-Level Parallelism from Laptops to Supercomputers. *Software X* **2015**, 1, 19-25.

35. Tribello, G. A.; Bonomi, M.; Branduardi, D.; Camilloni, C.; Bussi, G. PLUMED 2: New feathers for an old bird. *Comp. Phys. Comm*. **2014**, 185, 604-613.

36. Tiwary, P.; Parrinello, M. From Metadynamics to Dynamics. *Phys. Rev. Lett.* **2013**, 111, 230602.

37. APEX2 Version 2014.9−0; Bruker AXS Inc.: Madison, WI, 2007.

38. XSHELL, Version 6.3.1; Bruker AXS Inc.: Madison, WI, 2004.

39. Dolomanov, O. V.; Bourhis, L. J.; Gildea, R. J.; Howard, J. A. K.; Puschmann, H. OLEX2: a complete structure solution, refinement and analysis program. *J. Appl. Cryst.* **2009**, 42, 339-341.

40. Greenlee, A. J.; Wendell, C. I.; Cencer, M. M.; Laffoon, S. D.; Moore, J. S. Kinetic and Thermodynamic Control in Dynamic Covalent Synthesis. *Trends in Chem.* **2020**, 2, 1043-1051.

41. Zhang, Y.; Zheng, X. J.; Cao, N.; Yang, C. L.; Li, H. A Kinetically Stable Macrocycle Self-Assembled in Water. *Org. Lett.* **2018**, 20, 2356-2359.

42. Katritzky, A. R.; Oniciu, D. C.; Ghiviriga, I.; Barcock, R. A. 4,6-Bis-(N,N-dialkylamino)-s-triazines and 2,4,6-Tris-(N,N-dialkylamino)-s-triazines - Synthesis, NMR-spectra and Restricted Rotations. *JCS Perkins Trans 2* **1995**, 4, 785-792.

43. Amm, M.; Platzer, N.; Guilhem, J.; Bouchet, J. P.; Volland, J. P. Structural and conformational study of substituted triazines by N-15 NMR and x-ray analysis. *Magn. Res. Chem.* **1998**, 36, 587-596.

44. Amm, M.; Platzer, N.; Bouchet, J. P.; Volland, J. P. Structural and conformational study of substituted triazines by H-1 and C-13 NMR analysis. *Magn. Res. Chem.* **2001**, 39, 77-84.

45. Katritzky, A. R.; Ghiviriga, I.; Steel, P. J.; Oniciu, D. C. Restricted rotations in 4,6-bis- and 2,4,6-tris-(N,N-dialkylamino)-s-triazines. *JCS Perkins Trans 2* **1996**, 3, 443-447.

46. Birkett, H. E.; Harris, R. K.; Hodgkinson, P.; Carr, K.; Charlton, M. H.; Cherryman, J. C.; Chippendale, A. M.; Glover, R. P. NMR studies of exchange between triazine rotamers. *Magn. Res. Chem.* **2000**, 38, 504-511.

47. Capelli, R.; Menke, A. J.; Pan, H.; Janesko, B. G.; Simanek, E. E.; Pavan, G. M. Well-tempered Metadynamics Simulations Predict the Structural and Dynamic Properties of a Chiral 24-Atom Macrocycle in Solution. *ACS Omega* **2022**, *7*, 30291–30296.

48. De Riccardis, F. The Challenge of Conformational Isomerism in Cyclic Peptoids. *Eur. J. Org. Chem.* **2020**, 20, 2981-2994.

49. Baxter, N. J.; Williamson, M. P. Temperature dependence of H-1 chemical shifts in proteins. *J. Biomolec. NMR* **1997**, 9, 359-369.

50. Lloyd-Williams, P.; Sanchez, A.; Carulla, N.; Ochoa, T.; Giralt, E. Synthetic Studies on Threonines. The Preparation of Protected Derivatives of D-allo and L-allo Threonine for Peptide Synthesis. *Tetrahed.* **1997**, 53, 3369-3382.

51. Barducci, A.; Bonomi, M.; Parrinello, M. Metadynamics. *Wiley Interdiscip. Rev. Comput. Mol. Sci.* **2011**, 1, 826-843.

52. Laio, A.; Parrinello, M. Escaping free-energy minima. *Proc. Natl. Acad. Sci.* 2002, 99 (20), 12562-12566.